INVITED ARTICLE

Branislav M. Notaroš

Meteorological Electromagnetics

Optical and radar measurements, modeling, and characterization of snowflakes and snow.

We introduce the concepts, methodologies, and applications of meteorological electromagnetics with a focus on snow, which currently is the least understood component of the global water cycle. As "no two snowflakes are alike," the intricacies of snowflakes and snowfall are both truly fascinating and extremely challenging to measure, analyze, and predict. We describe a unique approach to the characterization of winter precipitation through the synergistic use of advanced optical instrumentation for in situ microphysical and geometrical measurements of ice and snow particles; image processing techniques to obtain the fall speed, size distribution, 3D shape (mesh), density, and effective dielectric constant of snowflakes; method of moments (MoM) scattering computations of precipitation particles; and state-of-the-art dual-polarization radars for the measurement of polarimetric scattering observables. We discuss the operations, observations, and analyses using this approach during a snow field campaign that took place in Colorado, United States, from 2014 to 2017, and we also introduce an international collaborative field program in association with the 2018 Winter

Digital Object Identifier 10.1109/MAP.2021.3054298
Date of current version: 1 March 2021

Olympics in South Korea. One goal of this article is to promote meteorological electromagnetics as an interdisciplinary field where nature, science, and technology meet in some of the most fascinating and rewarding ways and where many key areas of interest and endeavors of the antennas and propagation community play an indispensable role.

INTRODUCTION

There are many obvious keywords that directly associate electromagnetics to meteorology and atmospheric science, like weather radar, radar meteorology, remote sensing of the atmosphere, precipitation scattering, radio-wave propagation through the atmosphere, atmospheric electricity, and so on. This article coins the term "meteorological electromagnetics" as an interdisciplinary field covering electromagnetic scattering and propagation modeling; in situ and remote-sensing measurements of precipitation using electromagnetic waves of all frequencies, including optics; and the microphysical and electromagnetic characterization and analysis of atmospheric particles, precipitation, and phenomena.

Specifically, some of the topics within this multifaceted field are: the electromagnetic modeling, observation, and analysis of snow, rain, and hail; scattering methods, models, and simulations based on synthetic particles (hydrometeors) or in situ measured hydrometeor properties; microphysical in situ measurements and characterization of precipitation particles; ground-based, airborne, and satellite weather radar and radiometric systems; dual-polarization (polarimetric) and/or multiwavelength radar observations of precipitation; image processing and hydrometeor classification using machine learning and other approaches; modeling, measurement, and implications of electromagnetic wave propagation through snow, rain, and hail; and advanced in situ and remote-sensing instrumentation and systems for precipitation measurement and characterization.

Meteorological electromagnetics explores the theoretical, practical, and societal aspects of these and similar topics and all of their components and variations as well as their synergies and discusses their impact on weather forecasting, atmospheric science, and meteorological research. This article focuses on snow, which currently is the least understood component of the global water cycle. In line with the saying that "no two snowflakes are alike," there indeed is a huge natural variability of the shapes, sizes, internal compositions, densities, and "habits" of snow and ice particles, which is even more complex when combined with their extreme sensitivity to subtle changes in environmental conditions [1]–[4]. The intricacies of snowflakes and snowfall are both truly fascinating and extremely challenging to observe, measure, analyze, understand, and predict.

On the other hand, the importance of accurate and reliable observations, analyses, understanding, and forecasting of snow events to the economy, safety, and everyday life can hardly be overstated. In extreme conditions, such as heavy snowstorms or ice storms, winter precipitation can cause substantial damage and havoc. Generally, the impact of improved winter precipitation forecasts (amount, location, and timing) is of great importance to all travel modes used by the public, especially air travel and safety. The socioeconomic impacts of hazardous winter precipitation are often underestimated, and the benefits of improved winter forecasting are enormous [5]. Some examples of these benefits and impacts include better decisions regarding aircraft deicing and hazardous road conditions for transportation safety, improved airport operational efficiency, and better decision making by utilities and emergency managers.

In addition, snow research, for example, methods for the accurate estimation of snow rates (accumulation), is of great interest and value to the hydrology community. Snow research is also important for analyzing the impacts of snow on radio-wave propagation, such as the assessment and remedying of radio-wave propagation impairments due to snow, e.g., signal depolarization along earth-to-satellite links using polarization diversity at K_a- and Q-bands due to ice complexity (phase, shape, and orientation). Moreover, even when it is raining—not snowing—it is important to study the ice processes, as precipitation often originates through the ice phase as snow or melting snow to form rain. This is particularly important in the midlatitudes, where about 85% of surface precipitation is constituted by such snow turning to rain events [6].

A full as possible understanding of the geometrical, microphysical, and scattering properties of ice and snow hydrometeors is essential for the development of radar-based quantitative precipitation estimation (QPE) algorithms [7]–[9]. It is also critical for the establishment, validation, and improvement of microphysical parameterizations used in numerical weather prediction models. The geometrical parameters are based on measurements and/or estimations of 3D shapes or 2D projections in different planes of hydrometeors. The usual microphysical properties are type/habit, fall speed, mass, density, and effective dielectric constant (relative permittivity) of particles, along with the particle size distribution (PSD) [7]–[9]. The scattering properties include the reflectivity, scattering matrix, and polarimetric scattering observables [10], which are related to the geometrical and microphysical particle properties in a complex manner.

Surface in situ observations of geometrical and microphysical properties have been coupled with scattering measurements by means of scanning and vertically pointing radars to develop radar-based QPEs, e.g., radar-based retrieval of liquid equivalent snow rate and accumulation maps [7], [9]. They have also been used for determining diverse snowflake habits [11]. Scattering models of snowflakes and other hydrometeors have been informed and validated by in situ and remote-sensing

measurements [12]. Various schemes have been developed to classify ice particles [13] based on images from optical instruments [14], [15]. The accurate measurement and characterization of ice particle properties are also crucial for the development of numerical schemes that predict the microphysical properties of ice particles and for the advancement and execution of numerical models for simulations of ice clouds and frozen precipitation and of forecast models overall. This does not only result in more accurate and reliable weather forecasts but can also impact regional climate modeling and simulations as well as climate projections.

This article describes a unique approach to the characterization of winter precipitation through the synergistic use of advanced optical instrumentation for in situ microphysical and geometrical measurements of ice and snow particles; image processing methodology to characterize the fall speed, size, shape, and density of hydrometeors; MoM scattering computations of precipitation particles; machine learning for snowflake classification; and state-of-the-art dual-polarization radars for the remote sensing of winter precipitation and the measurement of fully polarimetric scattering observables [16]–[35].

We develop geometrical, microphysical, and scattering models of natural snowflakes and tie them with radar observations. We also perform comparative studies of snow types and habits from in situ measurements and radar data and analyze the microphysical characteristics of particles. We demonstrate that optical instrumentation for snowflake measurements, image processing techniques, and scattering models can be used to explain polarimetric radar observations and their links to the microphysical characteristics of snowflakes and ice precipitation, providing diagnostic and predictive assessments of underlining meteorological and atmospheric backgrounds and developments.

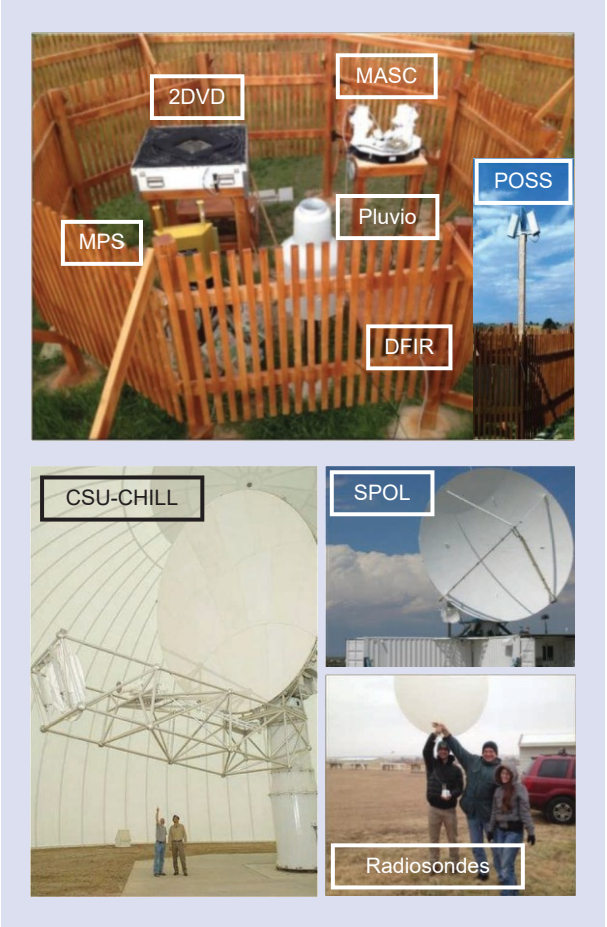

FIGURE 1. MASCRAD Snow Observation Field Site, near Greeley, Colorado, United States. Shown are the MASC, 2D video disdrometer (2DVD), Pluvio snow gauge, meteorological particle spectrometer (MPS), double fence intercomparison reference (DFIR) wind screen, precipitation occurrence sensor system (POSS), Colorado State University (CSU)-CHILL and National Center for Atmospheric Research (NCAR)-SPOL radars, and mobile sounding equipment for launching radiosondes with weather balloons for the measurement of various atmospheric parameters aloft.

IN SITU AND REMOTE-SENSING PRECIPITATION MEASUREMENT AND CHARACTERIZATION

We describe in situ surface measurements and remote sensing observations, followed by an analysis of winter precipitation within the multiangle snowflake camera (MASC) + Radar (MASCRAD) snow campaign [16]–[35]. The MASCRAD project involved the installation of a ground instrumentation site at the Easton Valley View Airport in La Salle, Colorado, depicted in Figure 1 [16]. Our main surface instrumentation included the MASC, 2DVD, POSS, Pluvio precipitation gauge, and MPS, as can be seen in Figure 1.

The site was operated under the coverage umbrellas of two state-of-the-art dual-polarization (horizontal and vertical) weather radars, the dual-frequency (S- and X-bands) CSU-CHILL radar and S-band NCAR-SPOL radar (Figure 1). Our main radar, CSU-CHILL, features a dual-offset Gregorian reflector antenna with exceptional polarization, directivity, and sidelobe characteristics [16]. The same antenna reflector system can be used with a two-frequency antenna feed to conduct dual-polarization measurements at both the S- and X-bands, one frequency at a time or simultaneously [36]. During snow events at the surface instrumentation site (Figure 1), including some periods before and after the storms, both radars conducted preprogrammed scan sequences based on customized strategies [16].

The POSS is a small, low-power (100 mW) continuous-wave X-band bistatic Doppler radar that measures the mean Doppler velocity and reflectivity (Z) with a measurement volume that is around 3 $m^3\ s^{-1}$ with peak gain located about 30 cm above the feed rectangular waveguide horn antennas [37]. The unit is mounted on a post about 3 m high (Figure 1). Its main feature is that it measures the reflectivity right at the in situ field site with surface instruments (within a few meters above ground level), thus avoiding the problems with scanning radars (such as the CSU-CHILL and NCAR-SPOL radars), where the sampling volume is much larger and typically hundreds of meters above the surface instruments. The Pluvio gauge is an automated weighing-type

gauge providing precipitation accumulation measurements and recording versus time. The MPS measures the PSD and fall speed of very small particles (as small as 50 *m*m in diameter), and it was used mostly for our rain observations [38].

The site also included mobile sounding equipment that allowed radiosondes to be launched into the atmosphere during intensive operational periods. As a radiosonde (suspended below a large balloon inflated with helium gas) rises vertically, its sensors measure various atmospheric parameters that are sent, along with GPS position data, by a radio transmitter to a sensitive tracking antenna on the ground. The received data are processed by a computer and can be viewed in real time. Sounding provided invaluable vertical profile high-resolution measurements of altitude, temperature, humidity, pressure, and winds. We launched radiosondes during (and before/after) major snowfall events at approximately 3 h intervals, as depicted in Figure 1. A surface Mesonet weather station provided similar readings at the ground.

We constructed the MASCRAD Field Site at the Easton Airport (Figure 1) in October 2014, as portrayed in Figure 2. To reduce the impact of horizontal surface wind on the precipitation measurements, especially in stronger wind conditions, the imaging instruments need to be placed inside a wind fence. A standard in accurate meteorological measurements is a "transparent" (not solid) double (two-layer) wind fence, a so-called DFIR wind screen [39]. A DFIR was constructed at Easton, and within it, the ground instruments were installed, as depicted in Figures 1 and 2. The shield provided very efficient wind suppression in all high-wind events during the MASCRAD campaign winter seasons [16]. The dish antenna was installed for an Internet connection to control the instruments remotely from the CSU campus.

OPTICAL INSTRUMENTATION FOR SNOWFLAKE MEASUREMENTS AND IMAGE PROCESSING

The MASC, illustrated in Figure 3(a), uses three cameras in the horizontal plane separated by 36° to capture high-resolution photographs of snowflakes or other frozen hydrometeors in freefall from three views, while simultaneously measuring their fall speed [11], [16]–[20], [24], [26]–[35]. For CSU's customized system, in Figure 3(b), the horizontal resolution is 35 μm, and the vertical resolution at a 1-m/s fall speed of particles is 40 μm. The virtual measurement area is 30 cm^2, and the measurement volume is ~200 cm^3/s. The instrument has two near-infrared emitter–receiver pair arrays positioned one above the other [Figure 3(a)], and as a particle falls through

FIGURE 2. The construction of a DFIR double wind fence and the MASC and 2DVD installation at the MASCRAD Easton site (Figure 1) by members of the Electromagnetics Lab at CSU (October 2014). This kind of field construction and instrument installation project, while not entirely sounding like graduate research, and not commonly undertaken directly by university research labs, is an excellent opportunity for students to gain an appreciation of the complexity of real-world research projects as well as some broader engineering skills, advance their rapport among the group and with their graduate advisor, and strengthen the morale of the group and the project team in tackling more conventional, and presumably more difficult, research tasks. Not less importantly, as can be observed from the photos, we had a lot of fun during these sunny October Colorado days and beautiful evenings.

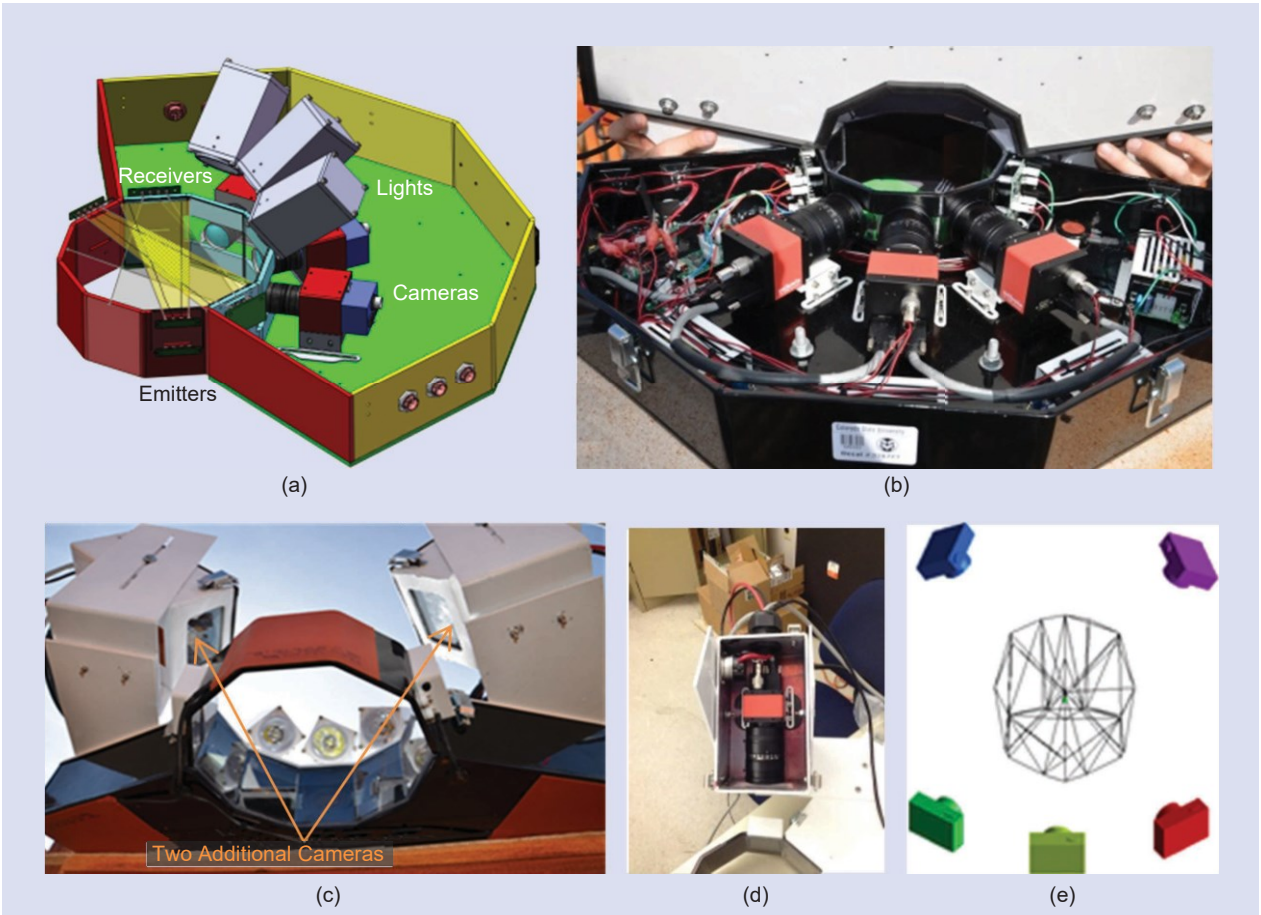

FIGURE 3. The MASC. (a) A 3D schematic of the three MASC cameras, three flashlights, and two (upper and lower) emitter–receiver near-infrared triggering arrays. (b) The CSU-MASC. (c) and (d) Adding two "external" cameras to the CSU-MASC to improve the 3D reconstruction of snowflakes. (e) A schematic showing the spatial positions of the cameras of the five-camera MASC and their field of view intersection, i.e., measurement volume [16], [17].

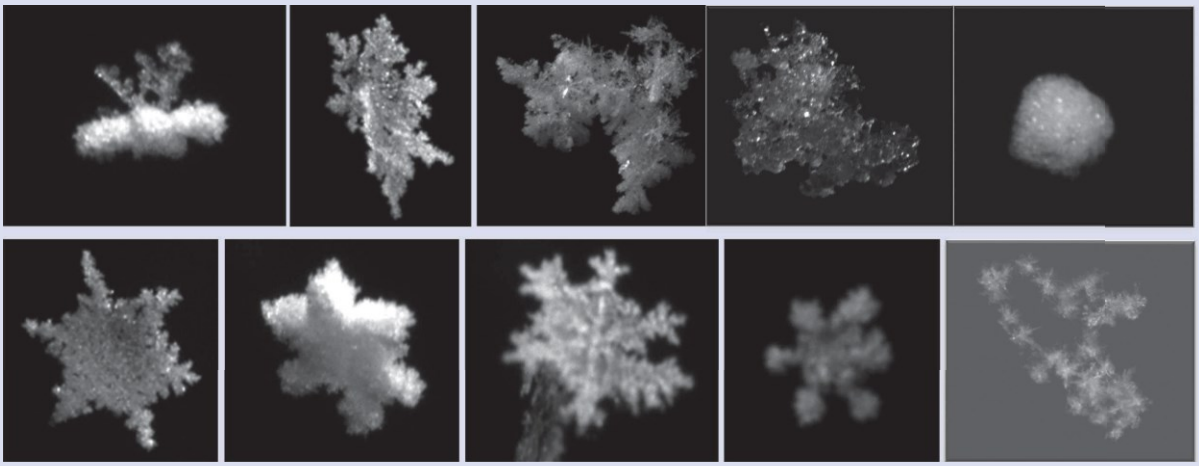

FIGURE 4. Illustrative examples of photographs of snowflakes with contrasting forms captured by the MASC (Figure 3) at the MASCRAD Field Site (Figure 1) during the MASCRAD winter campaigns [16].

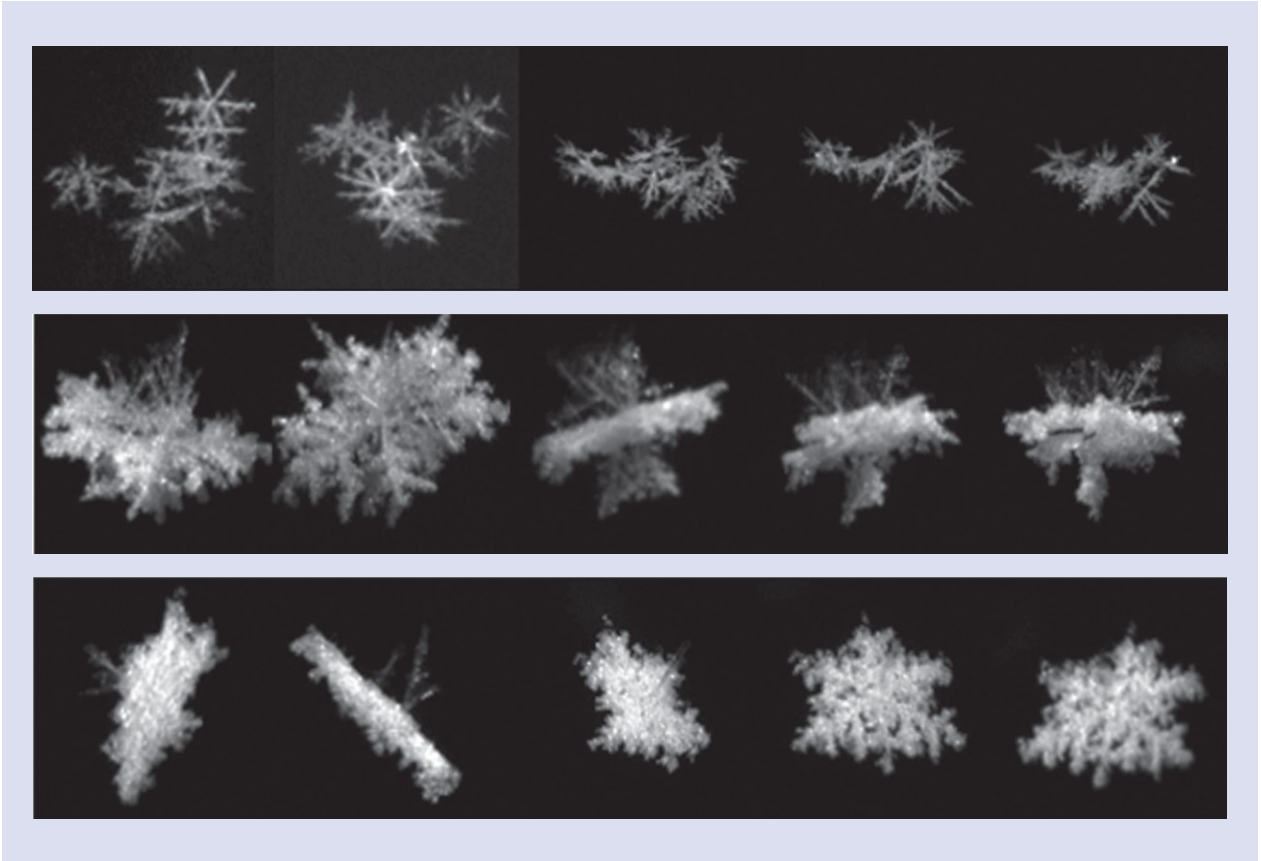

FIGURE 5. Photographs of three snow particles captured by the five-camera CSU-MASC in Figure 3(c) (each row is for a different snow example). Within each row, the five camera views are shown [17].

the lower array, it triggers all of the cameras. Additionally, the fall speed of a particle is obtained by simply dividing the distance between the two triggering arrays by the time it takes the particle to fall through between the two triggers.

The placement of the cameras in one plane with a small separation in viewing prevents realistic 3D shape reconstruction [17]. To remedy this, two cameras were added to the CSU-MASC, "externally" above the original cameras and at a 55° angle with respect to the horizon, as seen in Figure 3(c)–(e), to provide additional views [16], [17]. All five cameras collect images synchronously at a maximum triggering rate of 2 Hz. Figures 4 and 5 depict characteristic examples of MASC photographs of snowflakes collected during the MASCRAD project.

The 2DVD uses high-speed line-scan cameras to produce two mutually orthogonal contour images of a particle (Figure 1) [7], [28], [30], [32]. While the 2DVD's resolution for the horizontal dimension is by a factor of ~4 lower than that of the MASC, its sampling area is larger by a factor of ~3, and the measurement volume is ~50 times that of the MASC at 1-m/s fall speed. In addition, the 2DVD provides more accurate and robust measurements of the particle fall speed and PSD.

We have developed an image processing technique based on the visual hull method for the reconstruction of 3D shapes of snowflakes and other precipitation particles (or other objects) using the photographs captured by the MASC (Figure 3) or a similar multicamera instrument [17]–[19]. As illustrated in Figure 6, the reconstruction is based on the sets of MASC photographs of the same object (snowflake) in freefall (Figure 5) and the corresponding 2D silhouettes of the snowflake [17].

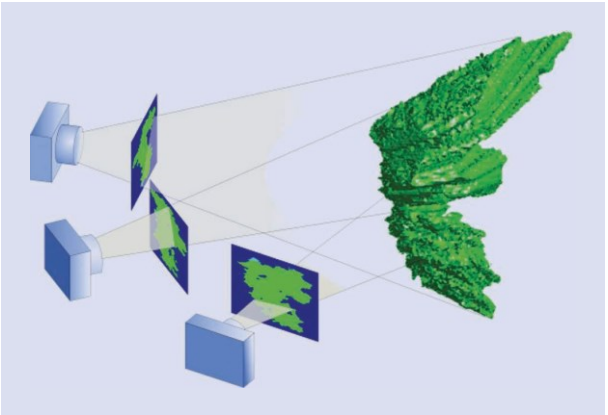

FIGURE 6. An illustration of the visual hull method with three cameras of the MASC in Figure 3(a) and (b). A 3D shape reconstruction of a snowflake is obtained by projecting and intersecting the corresponding silhouettes of the particle [17].

Figure 7 indicates that our method can provide accurate 3D shape reconstructions in cases where the actual geometries of the objects are known, namely, for 3D printed fake snowflakes dropped through the five-camera MASC [17]. Further, Figure 8 gives two examples of real snowflakes, where we observe an almost perfect reprojection of the reconstructed realistic and complicated shapes and compositions and excellent coverage of these 2D reprojections as silhouettes onto the original photographs of the snowflakes.

From a surface mesh obtained by the visual hull 3D reconstruction method, representing a realistic, complex 3D shape of a snow or ice particle, we are able to compute readily, for example, by numerical volume integration, the volume of the model. Combining it with the mass estimation from the fall speed measured by the MASC using Böhm's method

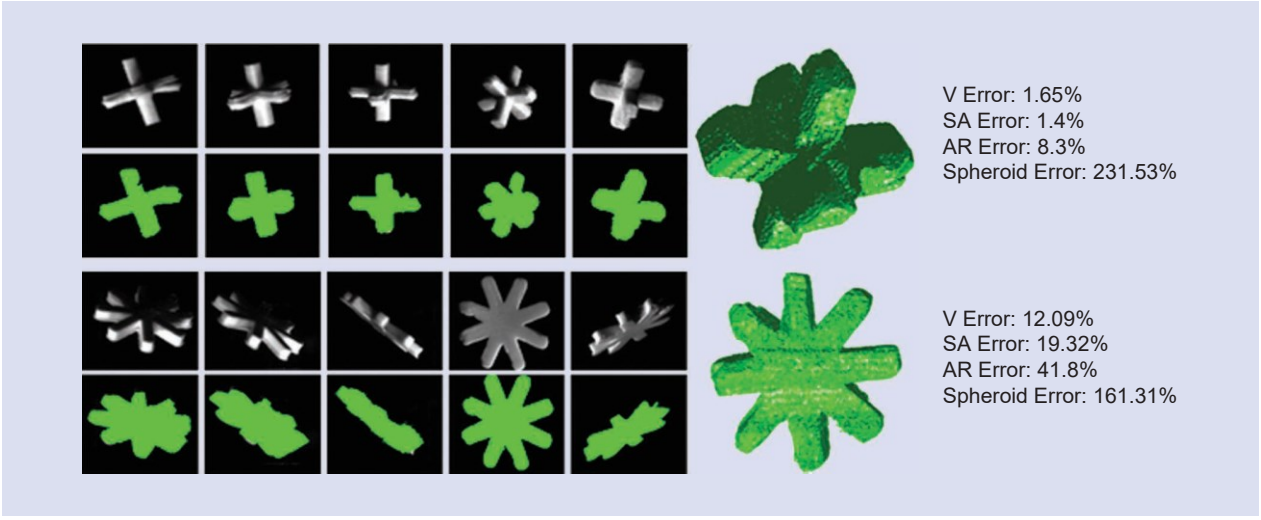

FIGURE 7. Two examples of visual hull reconstructions (see Figure 6) of 3D printed fake snowflakes and the corresponding photographs from the modified MASC system in Figure 3(c)–(e), along with the back projections of 3D reconstructed shapes onto the original 2D images. Percent errors of the volume (V), surface area (SA), and aspect ratio (AR) of the 3D reconstructions with respect to the known 3D CAD models are given as well. The error in V for the reconstructions of 3D printed fake snowflakes using spheroids (a conventional approach) is also shown [17].

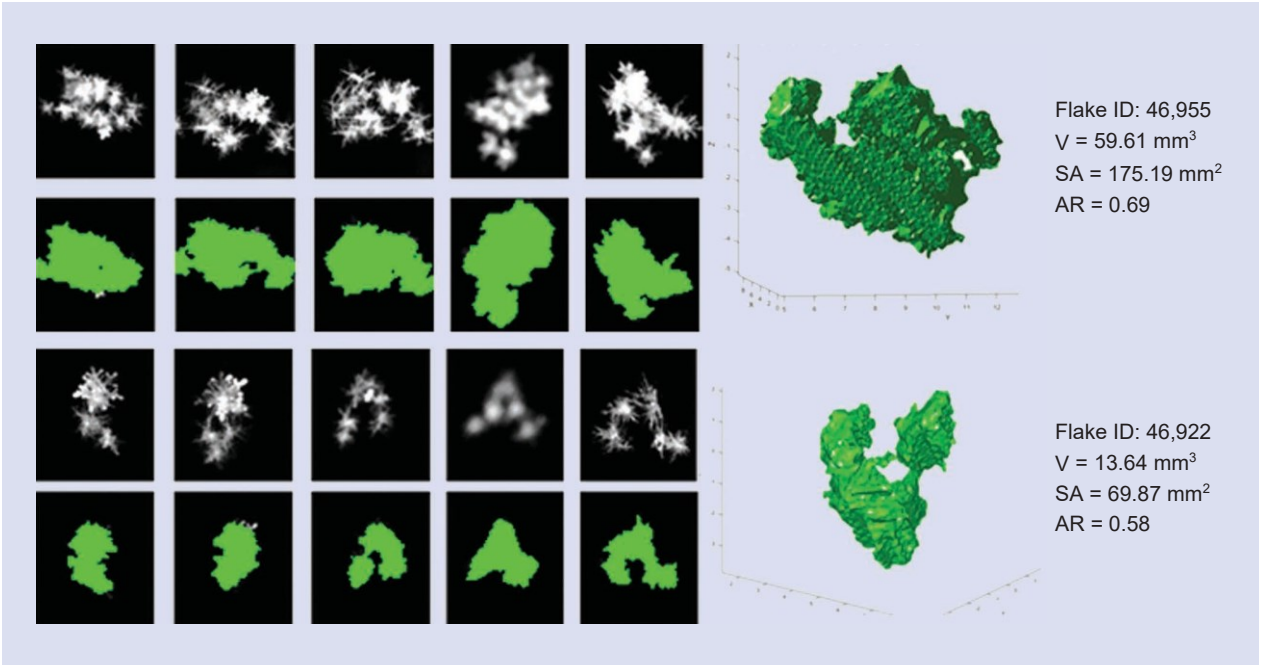

FIGURE 8. Two examples of 3D reconstructions with the visual hull method (see Figure 6) of snowflakes based on images recorded by the MASC [Figure 3(c)–(e)] at the MASCRAD site (Figure 1) during a snowstorm on 23 February 2015 [17].

[40], we then obtain the effective density of the hydrometeors. The density is finally used to estimate the effective dielectric constant, ε_r, of the particle, in accordance with the Maxwell-Garnett formula [41].

The 3D shape reconstructions (meshes) of snow particles by the visual hull method and the estimated dielectric constants are extremely valuable for microphysical characterizations of winter precipitation. We use them for realistic computation of "particle-by-particle" scattering matrices and dual-polarization radar observables, for studies of snow habits, for radar-based QPE, e.g., snow rate estimation, and for hydrometeor classification.

PRECIPITATION PARTICLE SCATTERING

The atmospheric science and meteorology communities are using the transition (T)-matrix method and the discrete dipole approximation (DDA) method for precipitation scattering computations [21]. The former approach invokes the T-matrix to relate incident and scattered waves expanded as vector spherical wave functions, and it runs extremely fast when it converges [21]. However, T-matrix tools are normally restricted to scatterers with rotationally symmetric shapes and smooth surfaces. The latter approach approximates a scatterer (particle) by volumetric cells represented by discrete electric dipoles, and it enables an analysis of particles of any shapes and material compositions [21]. However, the accuracy and convergence properties of the DDA method can be problematic, and the simulation can be prohibitively slow.

We have proposed and used an efficient and accurate computational electromagnetics approach to precipitation particle scattering analysis based on the higher-order MoM integral equation modeling [21]–[23], [42]–[45]. We use the surface integral equation (SIE) formulation in most cases, with volume integral equation modeling being invoked in the analysis of melting ice and similar inhomogeneous particles. This approach is much more broadly applicable than the T-matrix method and is 2–3 orders of magnitude faster than the DDA in some examples [21]. Furthermore, both the T-matrix and DDA solutions may not converge in cases of electrically large or geometrically complex particles [21]. Figure 9 portrays a simple illustration of a comparison of MoM-SIE, T-matrix, and DDA precipitation particle scattering calculations.

CLASSIFICATION OF SNOWFLAKES USING CONVOLUTIONAL NEURAL NETWORKS

The classification of precipitation, namely, deciding which of the several typical classes of winter hydrometeors the observed particles belong to, can enrich our understanding of polarimetric radar signatures of snow and advance QPE. The high-resolution photographs of snowflakes collected by the MASC are especially suitable for snowflake classification. Classifying particle types by visual inspection is not practical given the typical amounts of data captured by a deployed MASC in a snowstorm. There have been dramatic recent developments in machine learning, including techniques based on convolutional neural networks (CNNs).

We have developed a CNN method for the accurate and fast automatic classification of snowflakes using MASC images [24]. In a supervised machine learning fashion, we first perform a visual inspection to develop a training data set based on an established classification scheme. Our current scheme classifies the MASC images into five categories of snowflakes [13], namely, aggregate (AG), columnar crystal

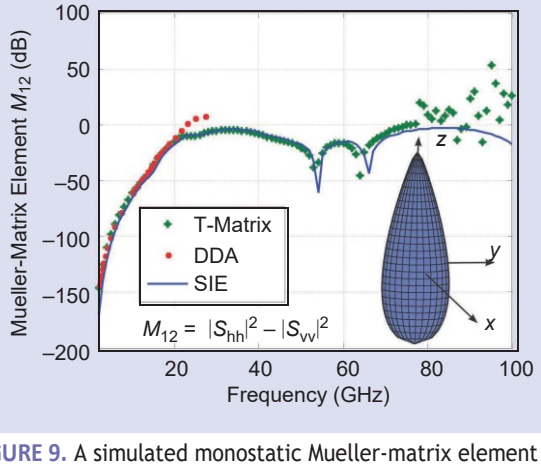

FIGURE 9. A simulated monostatic Mueller-matrix element M_{12} (defined in the inset) of a conical wet graupel. The length of the particle is 5 mm, the middle diameter is 1 mm, and the dielectric constant is $\varepsilon_r = 80 - j20$. The MoM-SIE model (mesh) shown in the inset yields convergent results at all frequencies. The DDA and T-matrix solutions above 27 and 76 GHz, respectively, do not converge for any predefined accuracy and computation time [21].

FIGURE 10. Five geometrical classes of snowflakes used for the classification of MASC images by means of CNNs [24].

(CC), graupel (GR), planar crystal (PC), and small particle (SP), as seen in Figure 10, and it can also estimate the degree of riming of snowflakes [24]. Riming is one of the crucial ice crystal growth processes (another one being aggregation) that is based on the collection of supercooled water droplets onto an ice crystal's surface, altering its shape, size, orientation, and density.

The high-resolution photographs of snowflakes collected by the MASC are especially suitable for snowflake classification.

As an example of the geometrical classification of snowflakes using the described CNN classifier, we consider snowfall cases on 23 – 31 December 2014 and 21–22 February 2015 at the MASCRAD Field Site (Figure 1). We performed network training with 900 iterations on +1,450 MASC photographs used as a training set. Figure 11 displays a confusion matrix obtained by the trained network when classifying + 400 snowflakes outside of the training data, with an intent to evaluate and demonstrate the so-called generalization of the network, namely, its ability to classify new (blind) data. Given in the bottom row are the percentage occurrences of correct classification and misclassification of the network on a per class basis for the five geometrical classes of snowflakes in Figure 10. The corresponding percentages for the out of class accuracy, that is, the ability of the network to not confuse an image within a class for something else, are sorted in the right-most column. Overall, the network achieved an excellent mean accuracy of 93.4%, given the small size of the data set [24].

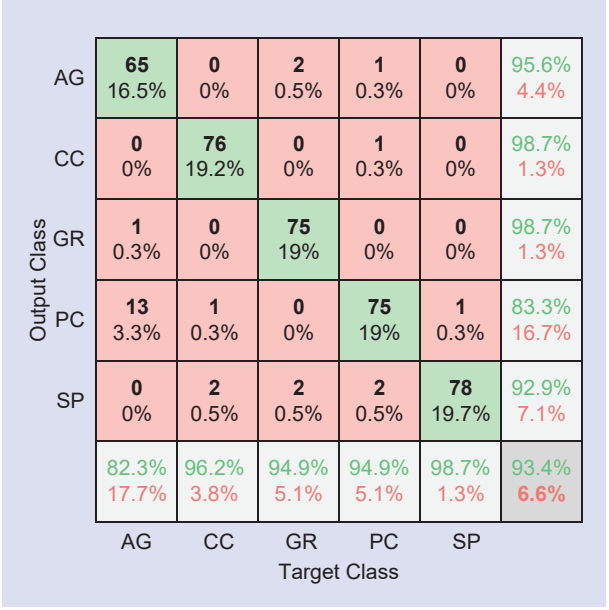

FIGURE 11. A confusion matrix for the described CNN classifier and geometrical classes of snowflakes in Figure 10 to illustrate the network's generalization on an example of 395 snowflakes from the 23-31 December 2014 and 21-22 February 2015 snow events at the MASCRAD Field Site (Figure 1). The target classes designate the actual input data, and the output classes represent the classification of the input data by the network. The numbers of images are shown in bold, with the corresponding percentages of the total number appearing immediately underneath. Diagonal boxes give correctly classified images, with the last one showing the overall network accuracy [24].

EXAMPLES OF MASCRAD OBSERVATIONS AND ANALYSES

The MASCRAD team performed operations and observations covering most of the snow events that occurred in the greater Easton Airport area (Figure 1) during the MASCRAD campaign winter seasons, from 2014 to 2017 [26]–[35]. Based on the forecasts sent by Dr. Andrew Newman of NCAR, a discussion would follow, and a decision was made whether or not to perform operations for the particular event. Then the specific plan and schedule of radar scans for both the CSU-CHILL and NCAR-SPOL radars were generated, and the operation of surface instrumentation at the MASCRAD Field Site (Figure 1) was checked. A detailed plan and schedule of launches of radio soundings (Figure 1) were also made and executed for each major event. Here, we present a sample of characteristic examples of results that are selected to illustrate MASCRAD observations and analyses.

The first example is a comprehensive analysis of an unusual winter graupel shower event on 16 February 2015 [30]–[32], which was supported by coordinated CHILL and SPOL radar data collection, sounding launches, and surface observations by optical instruments (Figure 1). The MASC (Figure 3) and 2DVD images showed small lump-type graupel particles (which, on the other hand, are not as unusual in the fall and spring seasons). The particle shapes and orientations were consistent with slightly, but consistently, negative values of the differential reflectivity, Z_{dr}, defined as the difference in (single-polarization) reflectivity, Z, at horizontal and vertical polarizations [10], observed by the radars.

A meteorological analysis of the sounding data indicated an environment that could facilitate the process of riming of pristine crystals (which were probably the predominant particle type in the higher-altitude region, with positive measured Z_{dr}) and their growth into graupel particles. Subfreezing temperatures and relatively humid conditions toward the ground enabled the formed graupel particles to survive as they fell to the site [30]. Figure 12 gives an illustrative sample of CSU-CHILL radar measurements and MoM-SIE polarimetric scattering simulations based on the MASC photographs collected during the event [16].

The second example is a case study of variations in snow crystal riming and ice particle habits as well as differential

reflectivity for a light snow event that occurred on 26–27 November 2015 at the MASCRAD Field Site (Figure 1) [33]–[35]. Figure 13 portrays a measured scatterplot in the Z_{dr} - Z plane using the CHILL X-band channel [36] for two distinct portions of the event on two days, respectively. For the entire event, the CHILL X-band Z (sample volume + 200 m) was in excellent agreement with Z measured by a POSS (Figure 1; sample volume few meters above surface). See [32] for another comparison of CHILL and POSS measurements (for the 11 November 2015 MASCRAD snow event).

Included in Figure 13 are also example MASC images from the two time periods considered [33]. During the early portion of the event, on 26 November 2015, we observed (Figure 13) higher Z levels (variations of +15 dB), indicating that the ice particles were larger, and reduced Z_{dr} (near 0 dB), meaning that, to the polarimetric radar, the particles appeared more "spherical" (for a sphere, $Z_{dr} = 0$ dB) as they descended to the ground. Indeed, the analysis of the MASC images demonstrated considerable particle riming and large fluctuations in fall orientation angles, which caused Z_{dr} values at near surface levels to reduce dramatically to +0 to 0.25 dB (note that the photograph from this period clearly signifies more riming on the crystal). In contrast, later in the event, on 27 November 2015, distinctly positive Z_{dr} values of + +2 to +3 dB were observed in a low Z environment, which was associated with the presence of much more pristine, very lightly rimed, and oriented single planar ice crystals (see the MASC image of 27 November) [33].

The third MASCRAD case is a major snow band passage on 21–22 February 2015, [16], [28], [29], [35]. The reflectivity (Z) values higher than 30 dBZ, recorded by both the CSU- CHILL (in the S-band mode) and NCAR-SPOL radars, were among the highest for all of the snowstorms observed during the

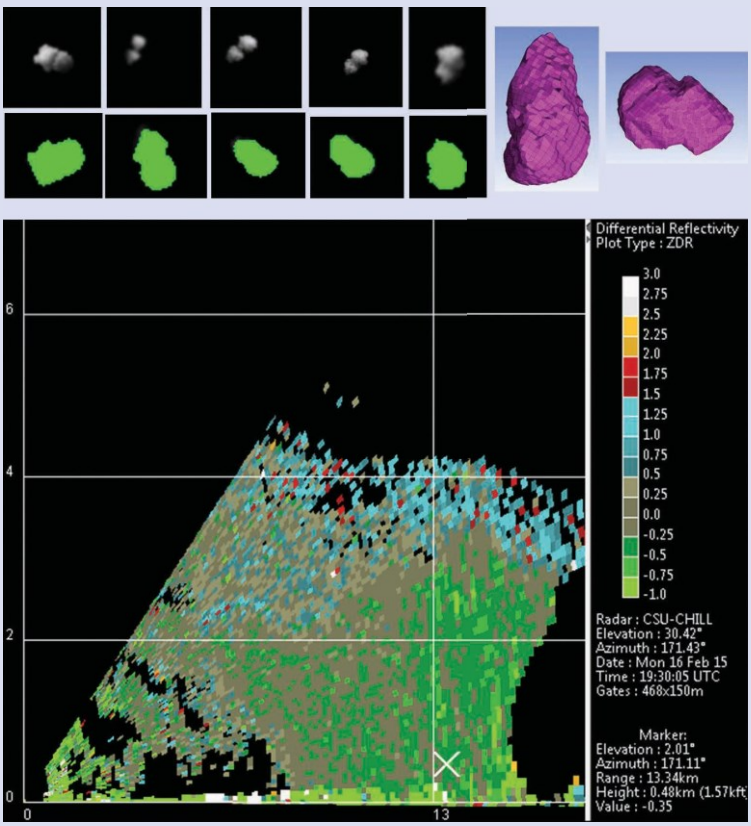

FIGURE 12. An illustration of CSU-CHILL radar (Figure 1) plots of differential reflectivity (Z_{dr}) and MoM-SIE polarimetric scattering calculations during an unusual winter graupel shower event on 16 February 2015. Radar measured Z_{dr} at the 12.92-km range at the MASCRAD Field Site (Figure 1) is −0.21 dB. The corresponding MoM-SIE result based on the photographs by the MASC (Figure 3) and the 3D shape reconstruction by the visual hull method (Figure 6) is $Z_{dr} = -0.15$ dB, with $f_r = 1.275 - j0.0003$ (obtained by Böhm's method and the Maxwell-Garnett formula) [16].

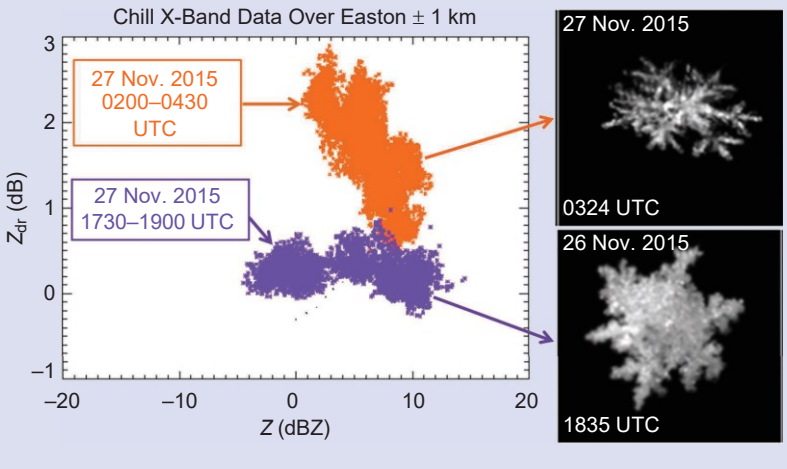

FIGURE 13. A scatterplot of CHILL radar (Figure 1) X-band reflectivity (Z) and differential reflectivity (Z_{dr}) data for two contrasting periods—featuring distinct variations in snow crystal riming and Z_{dr}—within a light snow event on 26-27 November 2015 at the MASCRAD site (Figure 1). Sample MASC images are shown for each of the two periods [33].

MASCRAD campaign winter seasons. Here, we illustrate the results of our developed method for determining the winter precipitation PSD from the MASC measurements [20] for this event. Figure 14 compares the average PSD from the three in-plane cameras of the MASC with the collocated 2DVD, measured during a period of time on 21 February 2015. We observe that the agreement is excellent for particle sizes (diameter of the volume-equivalent sphere) ① 4–5 mm, with a sampling error in the MASC at larger sizes being evident due to a much smaller sampling volume of the MASC. With collocated instruments, as in Figure 1, the high-resolution MASC can be used for the small size end of the PSD, while the poorer-resolution 2DVD can be used for the medium-to-large size end. Good agreement in the overlap region between 2 and 3 mm can be used to ascertain measurement accuracy [20].

The MASCRAD team performed operations and observations covering most of the snow events that occurred in the greater Easton Airport area during the MASCRAD campaign winter seasons, from 2014 to 2017.

2018 WINTER OLYMPICS INTERNATIONAL FIELD CAMPAIGN

As an example of a large field campaign that typically covers a larger area, involving myriad in situ optical and meteorological instruments at multiple surface instrumentation sites, a range of scanning and vertically pointing radars, and engaging a large number of institutions, usually as an international effort, we describe here a large coordinated international winter observation, nowcasting, and forecasting campaign that took place during and around the 2018 Winter Olympics in South Korea. This campaign, known as the International Collaborative Experiments for Pyeongchang 2018 Olympic and Paralympic Winter Games (ICE-POP 2018), lasted from 1 December 2017 through 31 March 2018, focusing on the measurement, physics, and improved prediction of heavy orographic snow in the Pyeongchang region of South Korea, where the Olympics was held.

The experiments were conducted under the auspices of the Korea Meteorological Administration and the World Meteorological Organization and involved 27 institutions and agencies from 12 countries in Asia, Europe, and North America. Figure 15 indicates the complexity of the Pyeongchang terrain, with a confluence of the continental and coastal regions and a mixture of significant orographic (mountains) and oceanic influences, which is of unique relevance for improving our understanding of severe winter weather over complex terrain and especially the impact of the ocean on snow for locations from the coastal area into the hills and high mountains.

In addition to multiple ICE-POP 2018 radar sites, there were five supersites for ground instruments; a partial list of the instruments for the main Mayhills supersite is depicted in Figure 15. Furthermore, as symbolically presented in the ICE-POP 2018 logo in Figure 16, the campaign involved aircraft measurements, ships, and satellite observations, e.g., the use of NASA Global Precipitation Measurement (GPM) satellite data.

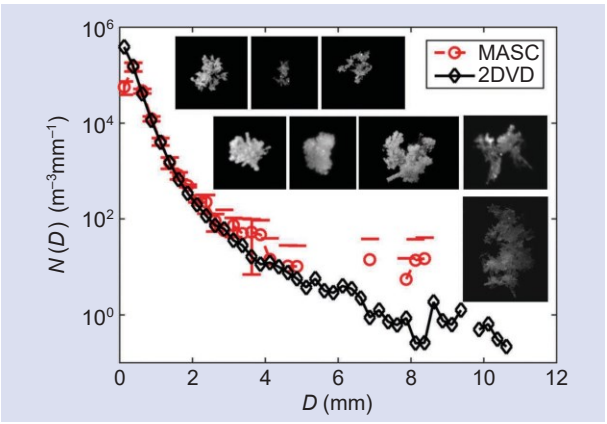

FIGURE 14. A comparison of the MASC mean PSD with the collocated 2DVD (Figure 1) PSD, with D being the particle apparent diameter (diameter of a sphere with the same volume as the snow particle) from the 2DVD, for a period of time during a major snow band passage event on 21–22 February 2015 at the MASCRAD Field Site (Figure 1). Samples of MASC images recorded during the storm are also shown [20].

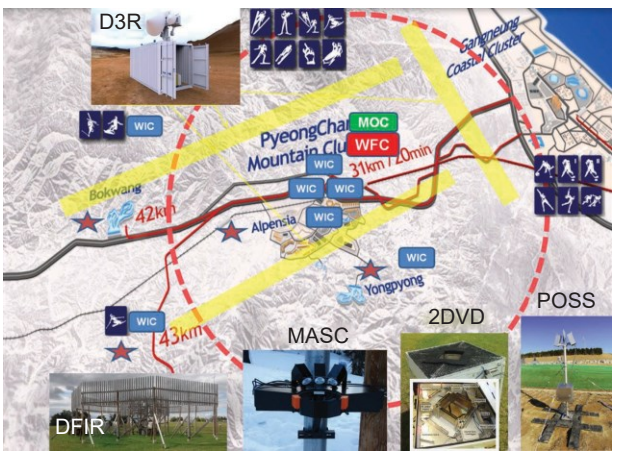

FIGURE 15. ICE-POP 2018 in South Korea, with a magnified picture of the Olympics venues, spread between the coastal area and the mountains. Some instruments at the main Mayhills supersite are shown (see the similarity with Figure 1) as well as NASA's dual-polarization, dual-wavelength (K_u, K_a)-band radar (D3R) [25].

Preparations for the ICE-POP 2018 campaign took several years. It was a truly international and interdisciplinary effort that includeds multiple scientific workshops, site visits, and planning meetings, as illustrated in Figure 16.

The ICE-POP 2018 observations included several "golden" snowfall events that provided an abundance of valuable measurements covering complementary observational data types moving gradually uphill from the coast to the mountains. The data on "golden" days combined dense and diverse surface, radar, and sounding measurements over the five supersites (Figure 15) for heavy snow, lighter snow, a rain–snow mix, and a transition of rain to snow at different locations and times. Some events involved satellite observations from GPM overpasses centered over the Olympics area. Analyses of the collected data, including comparisons of the observations to the results using weather prediction numerical models, will take many years, again as an international and interdisciplinary collaboration aimed at improving our understanding and prediction of orographic snowfall as well as the continental and coastal influences on it.

CONCLUSIONS

This article has introduced the concepts, methodologies, and applications of meteorological electromagnetics with an emphasis on snow and its intricacies, which make it extremely challenging to observe, analyze, and forecast. We have

FIGURE 16. Preparations for ICE-POP 2018. (a) An inspection of a 3D topographic model of the Pyeongchang mountains with Olympic Winter Games venues and a discussion of the locations of the ICE-POP 2018 supersites and radars on 22 March 2016. (b) A site survey of the Alpensia Ski Jumping Center supersite, 22 March 2016. (c) A site survey of the DaeGwallyeong Regional Weather Office supersite on 22 March 2016, with large snowflakes falling, like those during the "golden" snow event on 28 February 2018 during ICE-POP 2018. (d) The ICE-POP 2018 Observation Working Group Workshop on 24 March 2016 at the Lakai Sandpine Resort in Gangneung (a coastal part of the campaign area), South Korea. (e) Scientific and social exchanges with hard-to-match Korean hospitality for ICE-POP 2018 Observation Working Group members in an authentic historical Korean house in the Pyeongchang region.

described the state-of-the-art methods and technologies for in situ and remote-sensing winter precipitation measurement and characterization employed during the MASCRAD snow field campaign that took place in Colorado, United States, from 2014 to 2017, as well as during ICE-POP 2018 in South Korea.

With the advent and establishment of optical imaging instruments for in situ observations of winter precipitation as well as the rapid advances in radar polarimetry, there has been great progress made in QPE for snow. The MASC (together with the CHILL radar), which was at the heart of the MASCRAD snow campaign, captures images with sufficiently detailed resolution such that crucial geometrical features and microphysical properties can be obtained by an analysis of these images for complex hydrometeors and intricate snow crystals. The high-resolution photographs of snowflakes collected by the MASC are especially useful if used in conjunction with automated image processing techniques, e.g., the presented visual hull method for reconstruction of 3D hydrometeor shapes and machine learning techniques for snowflake classifications based on geometrical characteristics and riming degree, respectively.

With the advent and establishment of optical imaging instruments for in situ observations of winter precipitation as well as the rapid advances in radar polarimetry, there has been great progress made in QPE for snow.

For example, the 3D shape reconstructions (meshes) of hydrometeors enable realistic scattering computation of polarimetric radar measurables. The classification of snowflakes based on MASC images is becoming increasingly useful in explaining or modeling the fascinating polarimetric radar signatures in winter storms. Overall, both surface in situ observations of the geometrical and microphysical properties of snowflakes and scattering measurements by means of dual-polarization, and possibly multiwavelength, radar systems tied together are vital for the advancement of our understanding of snow, for the development of radar-based QPE algorithms for snowfall, and for the advancement of numerical winter weather forecast models and regional climate projections.

Finally, one goal of this article is to promote meteorological electromagnetics and its theoretical, practical, and societal aspects as an interdisciplinary and multifaceted field that invokes many key areas of interest and endeavors of the antennas and propagation community, such as scattering, propagation, computational electromagnetics, remote sensing, radar, radar antennas, optical measurements, meshing, image processing, machine learning, uncertainty quantification, and the design and development of microwave and optical in-situ and remote-sensing instrumentation and systems. Meteorological electromagnetics is a bridge between disciplines, bridging antennas and propagation/electromagnetics and atmospheric science/meteorology.

I hope that this article and the presented work have outlined the background, concepts, problems, and challenges of snow research and indicates some of the needs and opportunities for the engagement of the antennas and propagation community to help address these challenges. Some examples are: improving scattering models and simulations; the accurate estimation of the effective f_r of snowflakes; the rigorous correlation of in situ and remote-sensing measurements; advancing the retrieval of snow microphysics from multifrequency and/or dual-polarization radars; the design and employment of phased-array weather radars; and harnessing machine learning breakthroughs for in situ and radar-based precipitation estimation, classification, and prediction. Ideally, this might ignite future collaborations of the two communities in explorations and discussions where nature, science, and technology meet in some of the most fascinating and rewarding ways.

ACKNOWLEDGMENTS

This work was supported by the U.S. National Science Foundation under Grant AGS-1344862 and by NASA Precipitation Measurement Missions Science grant NNX16AE43G. The author would like to thank his collaborators and students on the MASCRAD project: Prof. V.N. Bringi, Patrick Kennedy, Dr. Gwo-Jong Huang, Dr. Merhala Thurai, Dr. Andrew J. Newman, Prof. GyuWon Lee, Dr. John Hubbert, Cameron Kleinkort, Dr. Elene Chobanyan, Dr. Sanja B. Manic´, and Adam Hicks. The author is also grateful to Prof. GyuWon Lee, principal investigator of ICE-POP 2018, for providing some of the diagrams and photos included in Figures 15 and 16.

AUTHOR INFORMATION

Branislav M. Notaroš (notaros@colostate.edu) is a professor and University Distinguished Teaching Scholar at Colorado State University, Fort Collins, Colorado, 80523-1373, USA. He is the author of several books and the recipient of 10 major national and international awards for research and teaching/education. He is a Fellow of IEEE.

REFERENCES

[1] H. R. Pruppacher and J. D. Klett, *Microphysics of Clouds and Precipitation* (Atmospheric and Oceanographic Sciences Library, vol. 18), 2nd ed. Berlin: Springer-Verlag, 2010.

[2] B. J. Mason, *The Physics of Clouds*. London: Oxford Univ. Press, 2010.

[3] W. Szyrmer and I. Zawadzki, "Snow studies. Part IV: Ensemble retrieval of snow microphysics from dual-wavelength vertically pointing radars," *J. Atmos. Sci.*, vol. 71, no. 3, pp. 1171–1186, 2014. doi: 10.1175/JAS-D-12-0286.1.

[4] K. G. Libbrecht, "Physical dynamics of ice crystal growth," *Annu. Rev. Mater.*, vol. 47, no. 1, pp. 271–295, 2017. doi: 10.1146/annurev-matsci-070616-124135.

[5] F. M. Ralph et al., "Improving short-term (0–48 h) cool-season quantitative precipitation forecasting: Recommendations from a USWRP workshop," *Bull. Amer. Meteor. Soc.*, vol. 86, no. 11, pp. 1619–1632, 2005. doi: 10.1175/BAMS-86-11-1619.
[6] P. R. Field and A. J. Heymsfield, "Importance of snow to global precipitation," *Geophys. Res. Lett.*, vol. 42, no. 21, pp. 9512–9520, 2015. doi: 10.1002/2015GL065497.
[7] G.-J. Huang, V. N. Bringi, D. Moisseev, W. A. Petersen, L. Bliven, and D. Hudak, "Use of 2D-video disdrometer to derive mean density–size and Ze–SR relations: Four snow cases from the light precipitation validation experiment," *Atmos. Res.*, vol. 153, pp. 34–48, Feb. 2015. doi: 10.1016/j.atmosres.2014.07.013.
[8] J. Leinonen, D. Moisseev, and T. Nousiainen, "Linking snowflake microstructure to multi-frequency radar observations," *J. Geophys. Res.*, vol. 118, no. 8, pp. 3259–3270, 2013. doi: 10.1002/jgrd.50163.
[9] A. J. Heymsfield, S. Y. Matrosov, and N. B. Wood, "Toward improving ice water content and snow-rate retrievals from radars. Part I: X and W bands, emphasizing CloudSat," *J. Appl. Meteor. Climatol.*, vol. 55, no. 9, pp. 2063–2090, 2016. doi: 10.1175/JAMC-D-15-0290.1.
[10] V. N. Bringi and V. Chandrasekar, *Polarimetric Doppler Weather Radar: Principles and Applications*. Cambridge, U.K.: Cambridge Univ. Press, 2001.
[11] T. J. Garrett, C. Fallgatter, K. Shkurko, and D. Howlett, "Fall speed measurement and high-resolution multi-angle photography of hydro-meteors in free fall," *Atmos. Meas. Tech.*, vol. 5, no. 11, pp. 2625–2633, 2012. doi: 10.5194/amt-5-2625-2012.
[12] O. O. Sy et al., "Impact of mass–size parameterizations of frozen hydrometeors on microphysical retrievals: Evaluation by matching radar to in situ observations from GCPEx and OLYMPEx," *J. Atmos. Oceanic Technol.*, vol. 37, no. 6, pp. 993–1012, 2020. doi: 10.1175/JTECH-D-19-0104.1.
[13] C. Magono and C. W. Lee, "Meteorological classification of natural snow crystals," *J. Fac. Sci., Hokkaido Univ., Series VII*, vol. 2, no. 4, pp. 321–335, 1966.
[14] J. Grazioli, D. Tuia, S. Monhart, M. Schneebeli, T. Raupach, and A. Berne, "Hydrometeor classification from two-dimensional video disdrometer data," *Atmos. Meas. Tech.*, vol. 7, no. 9, pp. 2869–2882, 2014. doi: 10.5194/amt-7-2869-2014.
[15] C. Praz, Y.-A. Roulet, and A. Berne, "Solid hydrometeor classification and riming degree estimation from pictures collected with a multi-angle snowflake camera," *Atmos. Meas. Tech.*, vol. 10, no. 4, pp. 1335–1357, 2017. doi: 10.5194/amt-10-1335-2017.
[16] B. M. Notaros et al., "Accurate characterization of winter precipitation using multi-angle snowflake camera, visual hull, advanced scattering methods and polarimetric radar," *Atmosphere*, vol. 7, no. 6, pp. 81–111, June 2016. doi: 10.3390/atmos7060081.
[17] C. Kleinkort, G.-J. Huang, V. N. Bringi, and B. M. Notaros, "Visual hull method for realistic 3D particle shape reconstruction based on high-resolution photographs of snowflakes in free fall from multiple views," *J. Atmos. Oceanic Technol.*, vol. 34, no. 3, pp. 679–702, Mar. 2017. doi: 10.1175/JTECH-D-16-0099.1.
[18] C. Kleinkort et al., "Visual hull method based shape reconstruction of snowflakes from MASC photographs," in *Proc. IEEE Int. Symp. Antennas Propag.*, July 19–24, 2015, Vancouver, BC, Canada, pp. 1122–1123.
[19] C. Kleinkort et al., "3D shape reconstruction of snowflakes from multiple images, meshing, dielectric constant estimation, scattering analysis, and validation by radar measurements," in *Proc. 37th Conf. Radar Meteorol., Amer. Meteor Soc.*, Sept. 14–18, 2015, Norman, OK.
[20] G.-J. Huang, C. Kleinkort, V. N. Bringi, and B. M. Notaros, "Winter precipitation particle size distribution measurement by Multi-Angle Snowflake Camera," *Atmos. Res.*, vol. 198, pp. 81–96, 2017. doi: 10.1016/j.atmosres.2017.08.005.
[21] E. Chobanyan, N. J. Sekeljic, A. B. Manic, M. M. Ilic, V. N. Bringi, and B. M. Notaros, "Efficient and accurate computational electromagnetics approach to precipitation particle scattering analysis based on higher-order method of moments integral equation modeling," *J. Atmos. Oceanic Technol.*, vol. 32, no. 10, pp. 1745–1758, Oct. 2015. doi: 10.1175/JTECH-D-15-0037.1.
[22] B. M. Notaros et al., "Computation of particle scattering matrices and polarimetric radar variables for winter precipitation using T-Matrix method, DDA method, and higher order MoM-SIE method," in *Proc. 37th Conf. Radar Meteorol., Amer. Meteor Soc.*, Sept. 14–18, 2015, Norman, OK.
[23] B. M. Notaros et al., "MoM-SIE scattering models of snow and ice hydrometeors based on 3D shape reconstructions from MASC images," in *Proc. Int. Appl. Comput. Electromagn. Soc. Conf. – ACES 2017*, Mar. 26–30, 2017, Firenze, Italy.
[24] A. Hicks and B. M. Notaros, "Method for classification of snowflakes based on images by a multi-angle snowflake camera using convolutional neural networks," *J. Atmospheric Oceanic Technol.*, vol. 36, no. 12, pp. 2267–2282, Dec. 2019. doi: 10.1175/JTECH-D-19-0055.1.
[25] G.-J. Huang, V. N. Bringi, A. J. Newman, G. Lee, D. Moisseev, and B. M. Notaros, "Dual-wavelength radar technique development for snow rate estimation: A case study from GCPEx," *Atmos. Meas. Techn.*, vol. 12, no. 2, pp. 1409–1427, 2019. doi: 10.5194/amt-12-1409-2019.
[26] B. Notaros et al., "Measurement and characterization of winter precipitation at MASCRAD snow field site," in *Proc. IEEE Int. Symp. Antennas Propag.*, July 19–24, 2015, Vancouver, BC, Canada, pp. 979–980.
[27] P. C. Kennedy et al., "Preliminary results from the multi-angle snowflake camera and radar (MASCRAD) project," in *Proc. 37th Conf. Radar Meteorol., Amer. Meteor Soc.*, Sept. 14–18, 2015, Norman, OK.
[28] W. Bang et al., "Microphysical characteristics analysis of three heavy snowfall events from the MASCRAD campaign in Greeley, Colorado, USA," in *Proc. URSI Asia-Pacific Radio Science Conf. – URSI AP-RASC 2016*, Aug. 21–25, 2016, Seoul, Korea, pp. 1555–1557.
[29] W. Bang et al., "The variability analysis of Z_{DR} and K_{DP} maxima zone through observation of three winter storms occurring in Colorado, USA," in *Proc. Int. Symp. Weather Radar and Hydrology – WRaH 2017*, Apr. 10–13, 2017, Seoul, Korea.
[30] V. N. Bringi, P. C. Kennedy, G.-J. Huang, C. Kleinkort, M. Thurai, and B. M. Notaros, "Dual-polarized radar and surface observations of a winter graupel shower with negative Z_{dr} column," *J. Appl. Meteor. Climatol.*, vol. 56, no. 2, pp. 455–470, Feb. 2017. doi: 10.1175/JAMC-D-16-0197.1.
[31] V. N. Bringi, B. Notaros, C. Kleinkort, G.-J. Huang, M. Thurai, and P. Kennedy, "Comprehensive analysis of an unusual winter graupel shower event recorded by an S-band polarimetric radar and two optical imaging surface instruments," in *37th Conf. Radar Meteorol., Amer. Meteor Soc.*, Sept. 14–18, 2015, Norman, OK.
[32] B. M. Notaros et al., "Snow precipitation measurement and analysis during MASCRAD winter observations," in *Proc. IEEE Int. Symp. Antennas Propag.*, June 26–July 1, 2016, Fajardo, Puerto Rico, pp. 2047–2048.
[33] P. Kennedy, M. Thurai, C. Praz, V. N. Bringi, A. Berne, and B. M. Notaros, "Variations in snow crystal riming and Z_{DR}: A case analysis," *J. Appl. Meteor. Climatol.*, vol. 57, no. 3, pp. 695–707, 2018. doi: 10.1175/JAMC-D-17-0068.1.
[34] B. M. Notaros, C. Praz, P. Kennedy, M. Thurai, A. Berne, and V. N. Bringi, "A case event analysis using multi-angle-snowflake-camera and CSU-CHILL X-band observations in Greeley, Colorado: Degree of riming and particle classification," in *Proc. 38th Conf. Radar Meteorol., Amer. Meteor Soc.*, Aug. 28–Sept. 1, 2017, Chicago, IL.
[35] B. M. Notaros et al., "MASCRAD Events: Observations and Analyses of Cases with Contrasting Hydrometeor Forms," in *Proc. IEEE Int. Symp. Antennas Propag.*, July 9–14, 2017, San Diego, CA, pp. 197–198.
[36] F. Junyent et al., "Transformation of the CSU-CHILL radar facility to a dual-frequency, dual-polarization Doppler system," *Bull. Amer. Meteor. Soc.*, vol. 96, no. 6, pp. 975–996, 2015. doi: 10.1175/BAMS-D-13-00150.1.
[37] B. E. Sheppard and P. I. Joe, "Performance of the precipitation occurrence sensor system as a precipitation gauge," *J. Atmos. Oceanic Technol.*, vol. 25, no. 2, pp. 196–212, 2008. doi: 10.1175/2007JTECHA957.1.
[38] M. Thurai et al., "Toward completing the raindrop size spectrum: Case studies involving 2D-video disdrometer, droplet spectrometer, and polarimetric radar measurements," *J. Appl. Meteor. Climatol.*, vol. 56, no. 4, pp. 877–896, Apr. 2017. doi: 10.1175/JAMC-D-16-0304.1.
[39] R. Rasmussen et al., "How well are we measuring snow: The NOAA/FAA/NCAR winter precipitation test bed," *Bull. Amer. Meteor. Soc.*, vol. 93, no. 6, pp. 811–829, 2012. doi: 10.1175/BAMS-D-11-00052.1.
[40] H. P. Böhm, "A general equation for the terminal fall speed of solid hydrometeors," *J. Atmos. Sci.*, vol. 46, no. 15, pp. 2419–2427, 1989. doi: 10.1175/1520-0469(1989)046<2419:AGEFTT>2.0.CO;2.
[41] J. C. Maxwell-Garnett, "Colors in metal glasses and in metallic films," *Phil. Trans. Roy. Soc.*, vol. 203, pp. 385–420, 1904.
[42] M. Thurai, S. Manic, M. Schönhuber, V. N. Bringi, and B. M. Notaros, "Scattering calculations at C-band for asymmetric raindrops reconstructed from 2D video disdrometer measurements," *J. Atmos. Oceanic Technol.*, vol. 34, no. 4, pp. 765–776, Apr. 2017. doi: 10.1175/JTECH-D-16-0141.1.
[43] S. B. Manic, M. Thurai, V. N. Bringi, and B. M. Notaros, "Scattering calculations for asymmetric raindrops during a line convection event: Comparison with radar measurements," *J. Atmos. Oceanic Technol.*, vol. 35, no. 6, pp. 1169–1180, June 2018. doi: 10.1175/JTECH-D-17-0196.1.
[44] M. Thurai, V. N. Bringi, A. B. Manic, N. J. Sekeljic, and B. M. Notaros, "Investigating rain drop shapes, oscillation modes, and implications for radiowave propagation," *Radio Sci.*, vol. 49, no. 10, pp. 921–932, 2014. doi: 10.1002/2014RS005503.
[45] M. Thurai, E. Chobanyan, V. N. Bringi, and B. M. Notaros, "Large raindrops against melting hail: Calculation of specific differential attenuation, phase and reflectivity," *Electron. Lett.*, vol. 51, no. 15, pp. 1140–1142, 2015. doi: 10.1049/el.2015.1564.